extinguishing metaflammation: mechanisms and therapeutic opportunities for immunological control of metabolic dysfunctions

Zande, H.J.P van der

Citation

Zande, H. J. P. van der. (2023, January 26). *extinguishing metaflammation: mechanisms and therapeutic opportunities for immunological control of metabolic dysfunctions*. Retrieved from https://hdl.handle.net/1887/3513911

CHAPTER 5

LKB1 signaling in dendritic cells controls whole-body metabolic homeostasis by limiting T helper 17 priming

Hendrik J.P. van der Zande, Eline C. Brombacher, Joost M. Lambooij,
Leonard R. Pelgrom, Anna Zawistowska-Deniziak, Thiago A. Patente, Graham A. Heieis,
Frank Otto, Arifa Ozir-Fazalalikhan, Maria Yazdanbakhsh, Bart Everts* and Bruno Guigas*

*These authors contributed equally to this study

Abstract

Obesity-associated metaflammation drives the development of insulin resistance and type 2 diabetes, notably through modulating innate and adaptive immune cells in metabolic organs. The nutrient sensor liver kinase B1 (LKB1) has recently been shown to control cellular metabolism and T cell priming functions of dendritic cells (DCs). Here, we report that hepatic DCs from high-fat diet (HFD)-fed obese mice display increased LKB1 phosphorylation and that LKB1 deficiency in DCs (CD11c$^{\Delta LKB1}$) worsened HFD-driven hepatic steatosis, systemic insulin resistance and glucose intolerance. Loss of LKB1 in DCs was associated with increased cellular expression of Th17-polarizing cytokines and increased hepatic CD4$^+$ IL-17A$^+$ Th17 cells in HFD-fed mice. Importantly, IL-17A neutralization rescued metabolic perturbations in HFD-fed CD11c$^{\Delta LKB1}$ mice. Mechanistically, disrupted metabolic homeostasis was independent of the canonical LKB1-AMPK axis. Instead, we provide evidence for involvement of the AMPK-related salt-inducible kinase(s) in controlling Th17-polarizing cytokine expression in LKB1-deficient DCs. Altogether, our data reveal a key role for LKB1 signaling in DCs in protection against obesity-induced metabolic dysfunctions by limiting hepatic Th17 differentiation.

Introduction

Obesity is associated with chronic low-grade inflammation, also known as metaflammation, where continuous overnutrition generates a self-sustained inflammatory loop in metabolic tissues that drives insulin resistance and type 2 diabetes (1). One of the hallmarks of metaflammation is the accumulation of myeloid cells in the main metabolic organs, *i.e.* white adipose tissue (WAT), liver and skeletal muscle (2). Macrophage-related cytokines such as tumor necrosis factor (TNF) and interleukin (IL)-1β were shown to inhibit insulin signaling (3, 4) and as such, macrophages are considered key players in the etiology of tissue-specific insulin resistance. However, dendritic cells (DCs) also accumulate in WAT and liver during obesity and are associated with metabolic dysfunctions. Indeed, depletion of the entire DC population or specific conventional DC (cDC) subsets in different genetic mouse models alleviates adipose tissue and/or hepatic inflammation, although the underlying mechanisms are incompletely understood (5-8).

DCs are specialized antigen presenting cells that govern T cell responses depending on the inflammatory and metabolic microenvironment. Moreover, modulation of T helper cell subsets in metabolic tissues has been shown to play a role in the control of immunometabolic homeostasis. For instance, T helper 2 (Th2) cells and regulatory T cells (Tregs) are enriched in lean, insulin sensitive WAT and contribute to maintenance of tissue-specific insulin sensitivity (9-11). On the contrary, Th17 cells accumulate in WAT and liver during obesity, and are associated with hepatic steatosis and insulin resistance (12-16). In addition, preventing CXCR3-dependent hepatic Th17 accrual and blocking IL-17A signaling using neutralizing antibodies both alleviated non-alcoholic fatty liver disease (NAFLD) (15, 16), suggesting an important contribution of hepatic Th17 cells to NAFLD severity. Although both DCs and T helper cell subsets in metabolic tissues have been associated with control of metabolic homeostasis, little is known about the regulation of DC-mediated T helper cell polarization in these organs during the development of obesity, and its impact on whole-body insulin sensitivity.

DC-mediated priming of Tregs and effector Th1, Th2 and Th17 cells is considered to be driven by metabolic rewiring of DCs in response to environmental cues, which controls co-stimulatory molecule and cytokine expression that shape T helper cell polarization (17). For example, *in vitro* Toll-like receptor (TLR)-activated mature DCs depend on glycolysis for fueling their anabolic demands, whereas quiescent DCs mainly rely on fatty acid oxidation and mitochondrial oxidative phosphorylation (18). As such, the obesity-induced changes in the metabolic organ microenvironment in which DCs reside may impact their T cell-polarizing capacities and contribute to metaflammation (19).

Among the bioenergetic sensors that regulate DC intrinsic metabolism and function *in vivo*, liver kinase B1 (LKB1) has recently received considerable attention (20-22). The tumor suppressor LKB1 is a serine/threonine kinase that can phosphorylate and activate AMP-

activated protein kinase (AMPK) and 12 other members of the AMPK-related family of protein kinases (23, 24), thereby controlling cell growth, survival, polarity and metabolism (25). In DCs, LKB1 was shown to be a critical regulator of effector T cell and Treg priming, thereby maintaining anti-tumor immunity (21, 22). We therefore hypothesized that LKB1 in DCs may connect the changing metabolic microenvironment during obesity to altered T cell priming, thereby impacting whole-body metabolic homeostasis.

In the present study, we investigated the role of LKB1 signaling in DC-mediated T helper cell priming in metabolic tissues and its impact on metabolic homeostasis. We demonstrate that obesity increased LKB1 phosphorylation in hepatic DCs, and that loss of LKB1 in DCs exacerbated metabolic dysfunctions by promoting AMPK-independent Th17 polarization in obese mice. Finally, we identify salt-inducible kinase(s) (SIK) as the possible LKB1 downstream mediator in repressing Th17-polarizing cytokine expression in DCs.

Results

Obesity induces DC activation in metabolic tissues and increases LKB1 phosphorylation in hepatic DCs

To investigate the role of dendritic cells (DCs) in whole-body metabolic homeostasis during obesity, male C57BL/6J mice were fed a high-fat diet (HFD) for 24 weeks, resulting in significant increases in body weight and fat mass when compared to low-fat diet (LFD)-fed control mice (Figure 1A-C). Using flow cytometry (Supplementary Figure 1), we assessed the frequency and phenotype of DCs in metabolic tissues from lean and obese mice. The number of DCs was found to be significantly increased in WAT but not in the liver from obese mice (Figure 1D-E). However, DCs from both tissues exhibited increased expression of activation markers (Figure 1F-G), a feature specific to metabolic tissues as activation status of DCs remained unchanged in the spleen (Supplementary Figure 2A). These changes in DC phenotypes were associated with alterations in the T helper cell pool in metabolic tissues. In eWAT, interferon (IFN)γ^+ Th1 cells were increased at the expense of IL-5$^+$ Th2 cells and FOXP3$^+$ regulatory T cells (Tregs), while in the liver we detected increased Th1 cells, IL-17A$^+$ Th17 cells and Tregs (Figure 1H-I). In line with unaltered expression of activation markers on splenic DCs, T cell cytokine expression in the spleen was largely unaffected in obese mice (Supplementary Figure 2B). These data suggest that the changing microenvironment in metabolic tissues during obesity alters DC activation and, consequently, DC-mediated T cell polarization.

As a bioenergetic sensor, LKB1 was recently shown to be a critical regulator of DC biology and T cell responses *in vivo* (20-22). We next investigated LKB1 signaling in spleen, eWAT and liver DCs by flow cytometry to determine its potential role in tissue-specific DC responses to

HFD. Interestingly, we found a marked increase in phosphorylation of Ser431-LKB1 specifically in hepatic DCs from obese mice, suggesting that LKB1 signaling within DC is altered during high-fat feeding, whereas Ser79-ACC phosphorylation, as a proxy for activity of the canonical LKB1 downstream target AMPK, was unchanged (Figure 1J-K; Supplementary Figure 2C). Together, these findings indicate that obesity-induced changes in the hepatic microenvironment may affect LKB1 signaling in DCs which is associated with altered hepatic T cell polarization.

LKB1 deficiency in DCs aggravates obesity-induced metabolic dysfunctions

To study the role of LKB1 in DCs in the context of obesity-induced metaflammation, we crossed *Stk11^flox/flox* mice to *Itgax^cre* mice to generate mice with CD11c-specific deletion of LKB1 as previously described (22). Male conditional knockout (CD11c$^{\Delta LKB1}$) and Cre$^-$ littermate control (CD11c^{WT}) mice were fed an HFD for 18 weeks (Figure 2A), which did not result in differences in body weight gain or body composition between genotypes (Figure 2B-E). Food intake, energy expenditure, and carbohydrate (CHO) and fatty acid (FA) oxidation were also not affected by loss of LKB1 in CD11c- expressing cells (Supplementary Figure 3). However, despite similar levels at baseline, CD11c$^{\Delta LKB1}$ mice developed higher fasting blood glucose levels than CD11c^{WT} littermates after 6 weeks on HFD, which was sustained throughout the experiment (Figure 2F). Furthermore, whole-body insulin resistance and glucose intolerance were worsened in CD11c$^{\Delta LKB1}$ mice, while glucose-induced insulin levels were similar (Figure 2G-I). Altogether, LKB1 in DCs is important for mitigating insulin resistance and restraining metabolic dysfunctions in mice during HFD-induced obesity.

Deletion of LKB1 in DCs promotes hepatic Tregs and Th17 cells and exacerbates hepatic steatosis

We next determined if the exacerbated metabolic dysfunctions observed in obese CD11c$^{\Delta LKB1}$ mice could be driven by tissue-specific immunometabolic changes. In eWAT, total leukocyte count and relative abundances of eosinophils, neutrophils, monocytes and CD11c/CD86-expressing macrophages were mostly unaffected (Supplementary Figure 4A-F). In line with our previous findings that LKB1-deficient DCs are more migratory (22), we found that the relative abundance of eWAT DCs was decreased in obese CD11c$^{\Delta LKB1}$ mice while frequencies of conventional DC (cDC) subsets between genotypes remained similar (Supplementary Figure 4G-H). As previous work revealed that LKB1-deficient DCs induced Tregs and effector Th17 cells mostly in lymphoid tissues of lean mice (21, 22), we next assessed whether these T helper subsets are affected in eWAT from obese CD11c$^{\Delta LKB1}$ mice. Despite similar CD4 T cell abundance, frequencies of FOXP3$^+$ Tregs and IL-17A$^+$ Th17 cells within the CD4 T cell pool were increased

in eWAT from obese CD11c^{ΔLKB1} mice, while IL-5$^+$ Th2 cells were not (Supplementary Figure 4I-L). However, when expressed as frequencies of total leukocytes, neither Tregs nor Th17 cells were significantly increased (Supplementary Figure 4M-N). Furthermore, adipocyte mean diameter and size distribution were not affected in obese CD11c^{ΔLKB1} mice (Supplementary Figure 4O-Q).
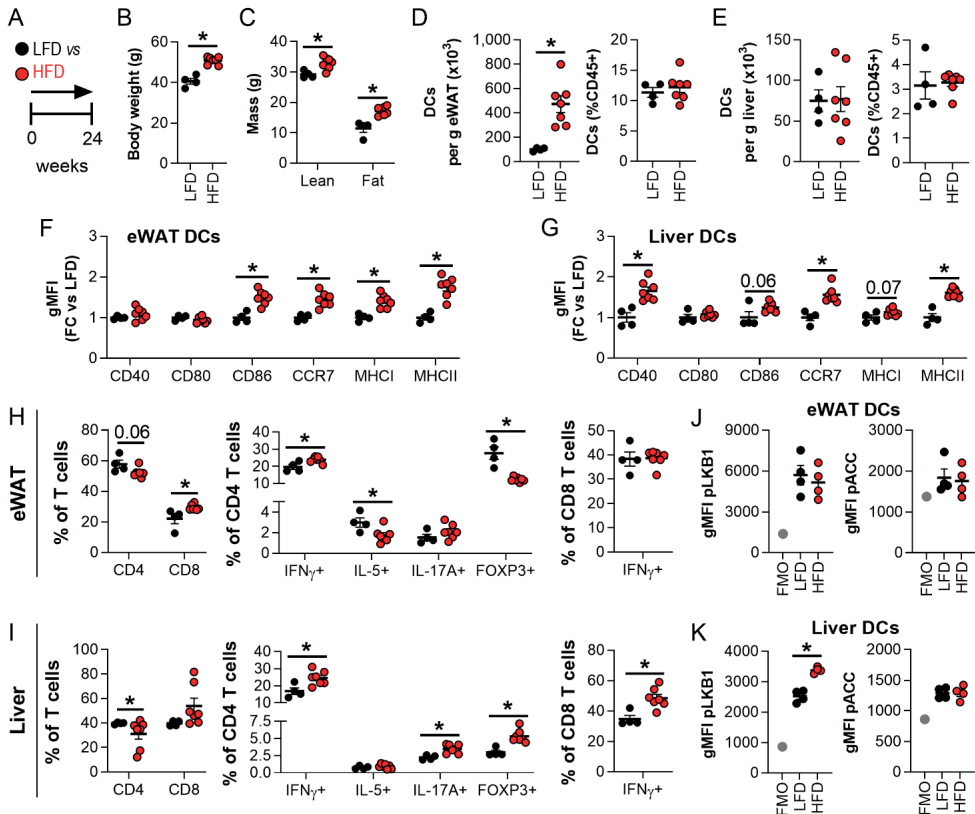

Figure 1. WAT and liver DCs are activated in obese mice. (**A**) Mice were fed a low-fat diet (LFD; black symbols) or a high fat diet (HFD; red symbols) for 24 weeks. (**B-C**) Body weight (*B*) and body composition (*C*) were measured at the end of the experiment. (**D-G**) At sacrifice, epididimal white adipose tissue (eWAT) and liver were collected and immune cells were isolated and analysed by flow cytometry. Absolute numbers of DCs per g tissue and frequencies of total leukocytes in eWAT (*D*) and liver (*E*). Relative expression of indicated DC markers by eWAT (*F*) and liver DCs (*G*). (**H-I**) Cells were restimulated with PMA/ionomycin in the presence of Brefeldin A for detection of intracellular cytokines, and were analysed by flow cytometry. CD4 and CD8 T cell, IFNγ$^+$ (Th1), IL-5$^+$ (Th2), IL-17A$^+$ (Th17) and FOXP3$^+$ (Treg) CD4 T cell and IFNγ$^+$ CD8 T cell percentages in eWAT (*H*) and liver (*I*). (**J-K**) eWAT and liver were immediately formaldehyde-fixed after collection and immune cells were isolated. Phosphorylated LKB1 (Ser431) and ACC (Ser79) were measured in DCs from eWAT (*J*) and liver (*K*) by flow cytometry. Full gating strategies are shown in Supplementary Figure 1. Results are expressed as means ± SEM. * P<0.05 vs LFD (n = 4-7 mice per group).
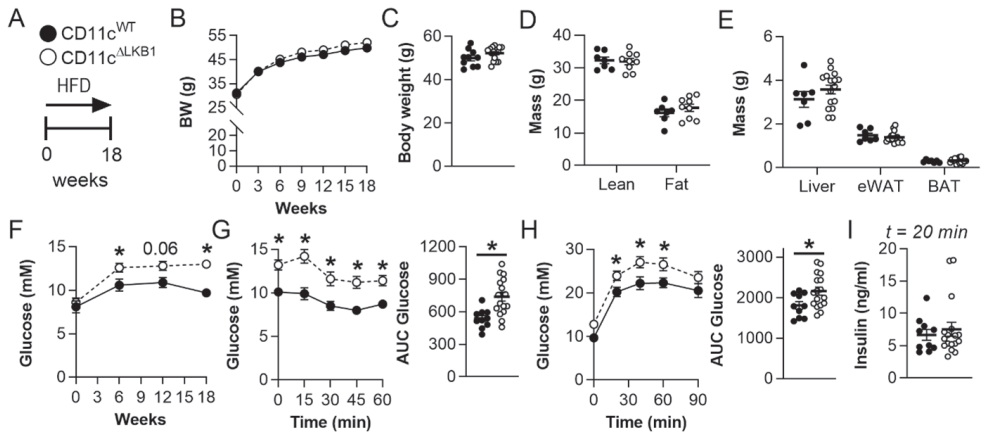
Figure 2. Deletion of LKB1 in DCs aggravates whole-body glucose intolerance and insulin resistance in obese mice. (**A**) CD11c^{WT} (black symbols) and CD11c$^{\Delta LKB1}$ (open symbols) mice were fed a HFD for 18 weeks. (**B-C**) Body weight was monitored throughout the experiment. (**D-E**) Body composition (*D*) and weights of liver, eWAT and BAT (*E*) were measured at the end of the experiment. (**F**) Fasting blood glucose was measured at the indicated weeks. (**G**) An i.p. insulin tolerance test was performed 1 week before sacrifice. Blood glucose levels were measured at the indicated time points and the AUC of the glucose excursion curve was calculated. (**H**) An i.p. glucose tolerance test (GTT) was performed 1 week before sacrifice. Blood glucose levels were measured at the indicated time points and the AUC of the glucose excursion curve was calculated. (**I**) Plasma insulin was measured at 20 minutes post glucose injection during i.p. GTT. Data shown are a pool of two independent experiments. Results are expressed as means ± SEM. * P<0.05 vs CD11c^{WT} (n = 7-17 mice per group).

In the liver, the abundance of total leukocytes, eosinophils, neutrophils, monocytes and macrophages, in addition to macrophage polarization, was unchanged in obese CD11c$^{\Delta LKB1}$ mice when compared to CD11c^{WT} littermates (Figure 3A; Supplementary Figure 5). As was also seen in eWAT, the frequency of DCs was reduced in the livers of CD11c$^{\Delta LKB1}$ mice, although the relative abundance of DC subsets remained similar. (Figure 3B-C). Strikingly, the proportions of liver CD4^{+} Tregs and Th17 cells were significantly increased in mice with LKB1-deficient DCs in comparison to LKB1-sufficient controls (Figure 3D-I). Moreover, the livers of CD11c$^{\Delta LKB1}$ obese mice exhibited enhanced hepatic steatosis when compared to WT littermates (Figure 3J-K). Consistent with this, hepatic triglyceride (TG) and total cholesterol (TC) levels were also increased (Figure 3L). Taken together, these results show that deletion of LKB1 in DCs induces a potent increase in Tregs and Th17 cells in the liver and exacerbates hepatic steatosis in obese mice.

IL-17A neutralization prevents exacerbated obesity-induced metabolic dysfunctions in mice lacking LKB1 in DCs

WAT and liver Th17 cells have consistently been linked to obesity-induced metabolic dysfunctions (13, 30), and hepatic steatosis in particular (12, 14-16). Accordingly, we observed elevated IL-17A-expressing CD4 T cells in the livers of obese mice lacking LKB1 in DCs, a feature that was associated with enhanced hepatic steatosis. Hence, to investigate the contribution of increased Th17 cells to worsened metabolic dysfunctions in CD11c$^{\Delta LKB1}$ obese mice, we treated them with either neutralizing antibodies for the Th17 effector cytokine IL-17A or isotype control during the first 6 weeks on HFD (Figure 4A). IL-17A neutralization did not impact body weight gain (Figure 4B-C) or hepatic Treg and Th17 cell abundances in CD11c$^{\Delta LKB1}$ mice (Supplementary Figure 6). However, IL-17A blockade led to significantly improved whole-body insulin sensitivity (Figure 4D) and reduced hepatic steatosis to comparable levels as CD11c^{WT} littermates (Figure 4E-G). Thus, increased IL-17A in CD11c$^{\Delta LKB1}$ mice plays a central role in promoting liver steatosis and metabolic dysfunctions during HFD-induced obesity. Altogether our findings suggest that LKB1 in DCs mitigates hepatic inflammation during the development of obesity by restraining Th17 priming.

To explore a direct role for LKB1-deficient DCs in promoting Th17 polarization, we sorted hepatic type 2 conventional DCs (cDC2s), the main CD4 T cell-priming subset shown to induce Th17 priming (31), from lean CD11c^{WT} and CD11c$^{\Delta LKB1}$ mice that were subcutaneously injected with Flt3L-secreting B16 melanomas to expand the *in vivo* DC pool (Figure 5A). Gene expression profiling validated knockout of *Stk11*, encoding LKB1, in hepatic cDC2s from CD11c$^{\Delta LKB1}$ mice (Figure 5C). While surface expression of activation markers on hepatic cDC2s was unchanged during homeostasis (Figure 5B), LPS-induced expression of the Th17-polarizing cytokines *Il6* and *Il1b* was enhanced in LKB1-deficient hepatic cDC2s when compared to controls, whereas *Il23a* was undetectable and *Tgfb1* unchanged (Figure 5C). These results show that LKB1 deficiency in DCs promotes production of cytokines, known to favor Th17 polarization, suggesting LKB1 in DCs restrains Th17 polarization by limiting IL-1β and IL-6 production.
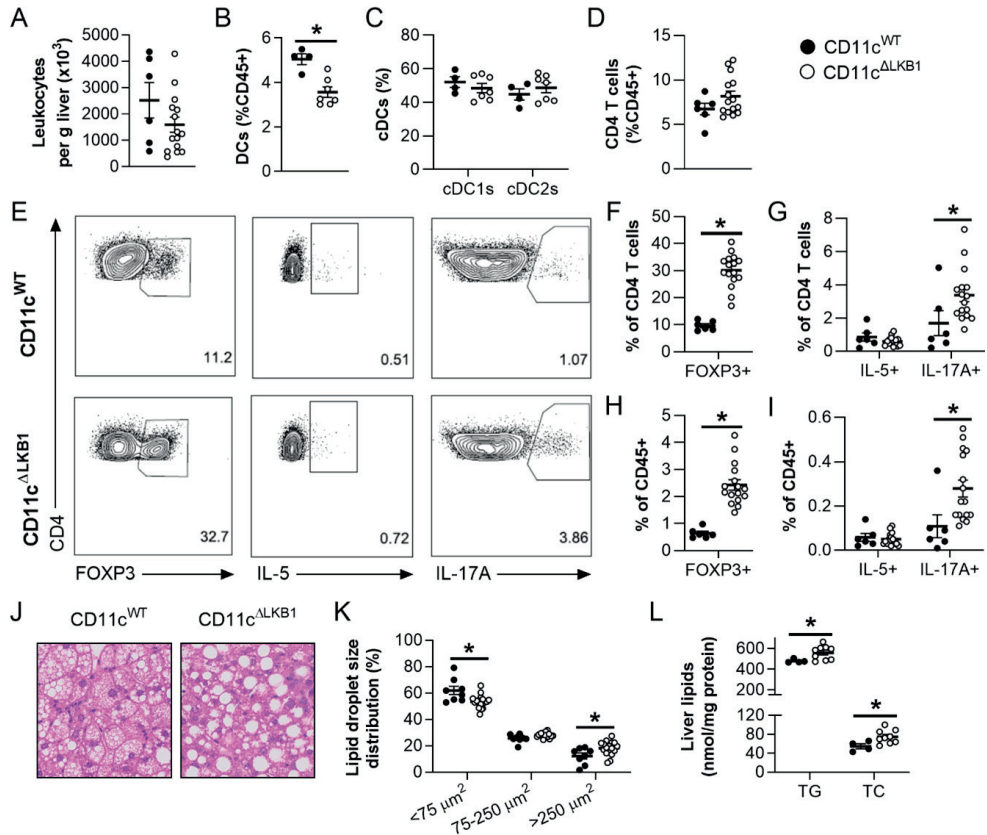
Figure 3. Obese CD11c$^{\Delta LKB1}$ mice are more susceptible to HFD-induced hepatic steatosis and have increased hepatic Treg and Th17 cells. CD11c^{WT} (black symbols) and CD11c$^{\Delta LKB1}$ (open symbols) mice were fed a HFD for 18 weeks. (**A-D**) At sacrifice, liver was collected and immune cells isolated. Total leukocytes per gram liver were quantified (*A*). Percentages of DCs (*B*), cDC subsets (*C*) and CD4 T cells (*D*) were determined by flow cytometry. (**E-I**) Liver leukocytes were restimulated with PMA and ionomycin in the presence of Brefeldin A for intracellular cytokine detection. Representative plots (*E*) and percentages of FOXP3$^+$ Tregs (*F,H*), IL-5$^+$ Th2 and IL-17A$^+$ Th17 cells (*G,I*) were determined as frequencies of CD4 T cells (*F,G*) or total leukocytes (*H,I*). (J) A part of liver was sectioned and H&E stained. (**K**) Lipid droplet sizes and size distribution were quantified from H&E-stained slides. (**L**) Hepatic triglyceride (TG) and total cholesterol (TC) contents were determined. Data shown are a pool of two independent experiments, except for B, C and L. Results are expressed as means ± SEM. * P<0.05 vs CD11c^{WT} (n = 6-17 mice per group for A, D-K; n = 4-9 mice per group for B, C and L).

The LKB1 downstream targets SIKs regulate Th17-polarizing cytokine expression in DCs independent of AMPK

Having demonstrated a role for LKB1 in DCs for preventing excessive obesity-induced metaflammation, we next investigated the signaling mediators downstream of LKB1 responsible for the altered Th17 priming function of DCs. The LKB1-AMPK axis represents a central node in the regulation of cellular energetics, where LKB1 promotes the downstream activation of AMPK though direct phosphorylation of its catalytic α-subunit (25). To assess whether AMPK is involved in the impaired metabolic homeostasis observed in CD11c^{ΔLKB1} obese mice, we generated CD11c^{ΔAMPKα1} mice, in which AMPKα1, the main α-subunit expressed by DCs (32), is deleted in these cells (22). We next fed them and their CD11c^{WT} littermates an HFD for 18 weeks (Supplementary Figure 7A). Surprisingly, none of the abovementioned detrimental immunometabolic changes observed in CD11c^{ΔLKB1} obese mice, *i.e.* increased fasting glucose levels, glucose intolerance, insulin resistance, and hepatic Tregs and Th17 cells, were recapitulated in HFD-fed CD11c^{ΔAMPKα1} mice (Supplementary Figure 7B-M). These data indicate that LKB1-deficiency promotes hepatic Th17 polarization in an AMPK-independent manner.

In addition to AMPK, LKB1 phosphorylates several other downstream AMPK-related kinases including MARK1-4, SIK1-3, NUAK1-2, SNRK and BRSK1-2 (23, 24). We therefore investigated which LKB1 target(s) may contribute to altering DC function by analyzing published datasets for their expression in total splenic DCs, as well as mature GM-CSF-elicited bone-marrow DCs (GMDCs; Supplementary Figure 8). The expression profiles were similar between primary splenic DCs and GMDCs, showing that all these kinases were expressed to a significant level with the notable exception of *Prkaa2* (encoding AMPKα2), confirming that only the catalytic AMPKα1 isoform is expressed by DCs (32), *Mark1* and the members of the BRSK family (Supplementary Figure 8A-B). Hence, we next determined their role in production of cytokine driving Th17 polarization by DCs. GMDCs were treated with inhibitors of MARK, SIK, NUAK and AMPK families prior to LPS stimulation, and intracellular levels of Th17-polarizing cytokines were assessed by flow cytometry. Largely consistent with liver-derived cDC2s from CD11c^{ΔLKB1} mice, LKB1-deficient GMDCs (Supplementary Figure 8C) displayed upregulated LPS-induced expression of pro-IL-1β, IL-6 and IL-23p19 when compared to wild-type GMDCs, whereas latency-associated peptide (LAP) expression, as a proxy for TGF-β production, was unchanged (Figure 5D). Strikingly, inhibition of SIKs, but not of the other LKB1 downstream kinases, recapitulated the cytokine profile of LKB1-deficient GMDCs (Figure 5D), identifying SIKs in DCs as potential regulators of Th17 polarization. Collectively, our data indicate that LKB1 signaling in DCs controls hepatic Th17 differentiation and metabolic homeostasis in obese mice, and we propose a role for SIK downstream of LKB1 in repression of Th17-polarizing cytokines.
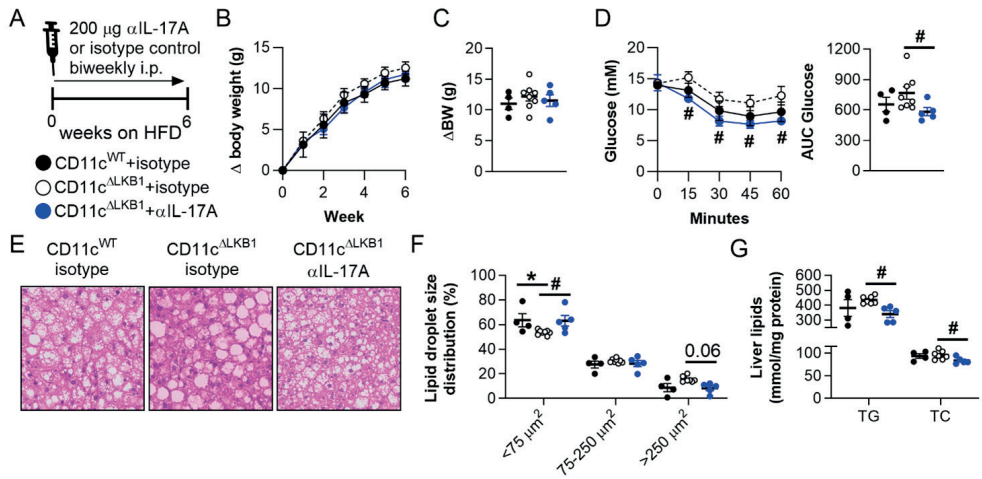
Figure 4. IL-17A neutralization rescued metabolic dysfunctions in CD11c$^{\Delta LKB1}$ mice. (**A**) CD11c^{WT} (black symbols) and CD11c$^{\Delta LKB1}$ mice were fed a HFD for 6 weeks while concomitant biweekly intraperitoneal treatment with IL-17A neutralizing antibodies (blue symbols) or isotype control (open symbols). (**B-C**) Body weight gain was monitored throughout the experiment. (**D**) An i.p. insulin tolerance test was performed during week 6. (**E**) At sacrifice, a piece of liver was sectioned and H&E stained. (**F**) Lipid droplet size distribution was quantified from H&E-stained slides. (**G**) Hepatic TG and TC content were determined. Data shown are a pool of two independent experiments. Results are expressed as means ± SEM. * P<0.05 vs CD11c^{WT}; # P<0.05 vs CD11c$^{\Delta LKB1}$ + isotype control (n = 4-8 mice per group).
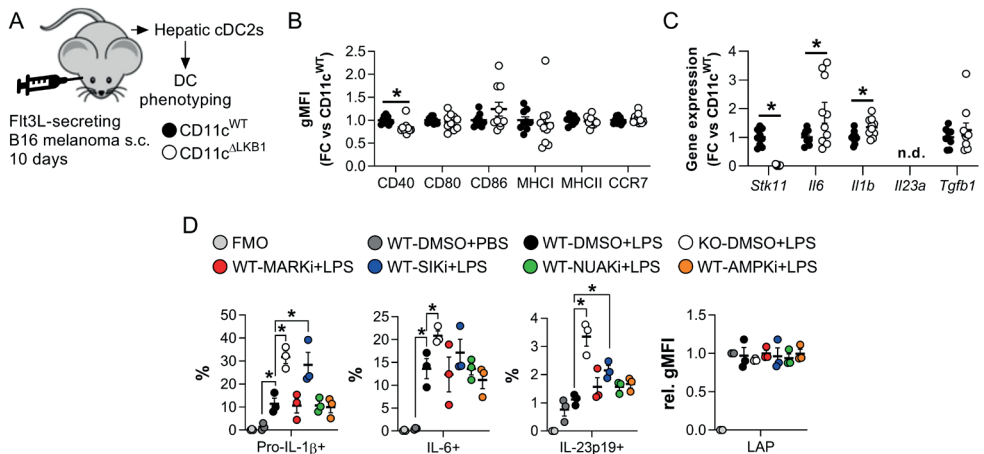

Figure 5. LKB1 deficiency increases Th17-polarizing cytokines expression in DCs, which is mediated through its downstream target SIK. (**A-C**) CD11c^{WT} (black symbols) and CD11c$^{\Delta LKB1}$ (open symbols) mice were subcutaneously injected with Flt3L-secreting B16 melanomas to expand the DC pool. After 10 days, hepatic cDC2s were FACS sorted for DC phenotyping (*A*). Expression

▲**Figure 5. Legend (Continued)**

of indicated DC markers was measured by flow cytometry (*B*). Expression of indicated genes was measured by RT-qPCR after *ex vivo* overnight LPS stimulation (*C*). (**D**) GM-CSF cultured bone marrow-derived DCs (GMDCs) from CD11c^{WT} (WT) mice were treated with inhibitors targeting LKB1 downstream targets MARKs, SIKs, NUAKs and AMPK for 2 h, before LPS stimulation in the presence of Brefeldin A for 4 h and compared with CD11c$^{\Delta LKB1}$ GMDCs (KO). Pro-IL-1β, IL-6, IL-23p19 and LAP-expressing GMDCs were quantified by intracellular cytokine staining/flow cytometry. Data shown are a pool of three experiments. Results are expressed as means ± SEM. * P<0.05 vs CD11c^{WT} or as indicated (n = 9-10 mice per group for A-C; n = 3 biological replicates per group for D).

Discussion

The bioenergetic sensor LKB1 was recently shown to be a critical regulator of DC metabolism, activation and T cell priming functions (20-22). Whether LKB1 signaling in DCs links the changing immunometabolic microenvironment during obesity with altered DC function and ultimately whole-body metabolic dysfunctions remained unclear. Here, we report that obesity increased LKB1 phosphorylation in hepatic DCs. Deletion of LKB1 from DCs aggravated HFD-induced insulin resistance and hepatic steatosis, and increased hepatic Tregs and Th17 cells in obese mice. These immunometabolic defects were restored by neutralizing the Th17 effector cytokine IL-17A, uncovering a role for LKB1 in restraining DC-mediated pathogenic Th17 cell differentiation, thereby controlling whole-body metabolic homeostasis.

Although DCs accumulate in WAT and liver during obesity and contribute to whole-body insulin resistance (5-8), the underlying mechanisms are incompletely understood. Indeed, obese *Flt3l$^{-/-}$* mice lacking DCs and *Ccr7$^{-/-}$* mice with impaired DC migration displayed reduced metaflammation and insulin resistance suggesting they have a central role in the development of metabolic dysfunctions (6, 7). Here, we report that DCs from eWAT and liver, but not spleen, of obese mice display increased expression of activation markers, indicating that the obesity-induced changes in the metabolic tissue microenvironment enhance DC activation. Interestingly, both eWAT and liver DCs from obese mice expressed higher levels of CCR7, suggestive of increased migration to draining lymph nodes where they can prime inflammatory T cells. Consistent with an increased proinflammatory activation profile of the DCs, we found that obesity altered the CD4 T helper cell pool in eWAT and liver, but not spleen, favoring Th1 cells at the expense of Th2 cells and Tregs in eWAT, and increasing Th1 cells, Th17 cells and Tregs in the liver. Some of these obesity-induced changes in T helper subsets in metabolic tissues have been reported previously (11, 16). Moreover, XCR1$^+$ type 1 conventional DCs (cDC1s), efficient at cross-presenting antigens to CD8 T cells, were reported to increase hepatic steatosis and contribute

to liver pathology, which was associated with inflammatory T cell reprogramming in the liver-draining lymph nodes (8). Congruent with this, we found increased HFD-induced IFNγ⁺ CD8 T cells in the liver, most likely resulting from increased cDC1-mediated priming.

In addition to increased DC activation and altered T cell priming in metabolic tissues, we observed a significant increase of Ser431-LKB1 phosphorylation in hepatic DCs of obese mice. LKB1 is phosphorylated at Ser431 by protein kinase C ζ (PKCζ) (33), p90 ribosomal S6 kinase (p90-RSK) and cAMP-dependent protein kinase A (PKA) (34). Although the exact consequence of phosphorylation at this site remains unclear, the residue corresponding to murine Ser431 is conserved in all organisms, suggesting that its phosphorylation may play a role in modulating LKB1 signaling. Despite a lack of a phenotype and normal AMPK activation in knock-in mice carrying a homozygous Ser431 to alanine mutation in LKB1 (35), it has been suggested that Ser431 phosphorylation could promote nuclear export of LKB1 and phosphorylation of some of its cytoplasmic substrates (33, 36).

Interestingly, Ser431-LKB1 phosphorylation was unchanged in splenic and eWAT DCs, indicating that obesity-induced changes in the hepatic microenvironment may specifically alter LKB1 signaling in liver-associated DCs and change its effector functions. Obesity induces persistent changes in the gut microbiota, and endotoxemia through increased gut permeability (37). As a result, the gut and serum metabolome are altered (38, 39), promoting NAFLD pathogenesis through a gut-liver axis (40). Since LPS injection has been reported to acutely increase Ser431-LKB1 phosphorylation in whole lung and liver lysates, and in immortalized Raw264.7 macrophages (41), one may hypothesize that obesity-induced endotoxemia might contribute to increased pLKB1 levels in hepatic DCs from obese mice. Of note, in Raw264.7 macrophages, LPS-induced Ser431-LKB1 phosphorylation suppressed NF-κB signaling, suggesting that increased pLKB1 in hepatic DCs from obese mice may serve as a feedback mechanism to keep inflammation in check. In addition, butyrate, a short-chain fatty acid produced by commensal bacteria that metabolize indigestible fiber, was recently shown to increase Ser431-LKB1 phosphorylation in HepG2 hepatocytes (42), providing conceptual evidence that gut metabolites may alter LKB1 phosphorylation in liver-resident cells. Yet, the underlying mechanisms by which LKB1 signaling is selectively modulated in hepatic DCs during obesity remain to be identified.

Deletion of LKB1 from DCs increased hepatic Tregs and Th17 cells in obese mice. Though predominantly focused on adipose tissue, the role of Tregs in the regulation of metabolic homeostasis has become controversial over recent years. Seminal work revealed that adipose tissue Tregs are lost during obesity (11, 43), and replenishing the Treg pool through IL-33 treatment or adoptive transfer reduced adipose tissue inflammation and improved metabolic homeostasis (44, 45). However, aging-associated insulin resistance is

ameliorated after depletion of adipose tissue Tregs (46), and deletion of the insulin receptor, IL-10 and the transcription factor Blimp1 from Tregs all prevented insulin resistance, in part through promoting adaptive thermogenesis (47, 48). We found a trend for increased adipose tissue Tregs in CD11c$^{\Delta LKB1}$ mice, yet eWAT weight, adipocyte size distribution, BAT weight and energy expenditure were unchanged, excluding a role for adaptive thermogenesis in the metabolic phenotype of CD11c$^{\Delta LKB1}$ mice. Hepatic Tregs were rather reported to control hepatic inflammation and inhibit NASH development (49). In addition, we clearly demonstrate that neutralizing the Th17 effector cytokine IL-17A rescued the metabolic perturbations in HFD-fed CD11c$^{\Delta LKB1}$ mice, indicating an important role for Th17 cells in explaining the metabolic phenotype of obese CD11c$^{\Delta LKB1}$ mice.

Indeed, obesity-induced hepatic Th17 cells and IL-17A signaling are consistently reported to impair insulin sensitivity and promote hepatic steatosis (12-16). Th17 differentiation is dependent on the cytokines IL-6, TGFβ, IL-1β and IL-23 (50, 51), but different combinations can lead to different degrees of pathogenicity. In the context of experimental autoimmune encephalitis, IL-6 and TGFβ-induced Th17 cells were not pathogenic, whereas IL-6, IL-1β and IL-23 induced Th17 cells were pathogenic (52, 53). Furthermore, development of Th17 cells *in vivo* is dependent on SIRPα/CD172a expression on DCs (31, 54), a marker of cDC2s that efficiently prime CD4 T cells. We previously showed that LKB1-deficient splenic cDC2s produced higher levels of IL-6 (22). In addition, others showed that mRNA expression of *Il6*, *Tgfb2* and *Il23a* tended to be increased in LKB1-deficient total splenic DCs compared to WT DCs, whereas *Tgfb1* and *Tgfb3* were decreased or similar (21). Moreover, increased Th17 priming by LKB1-deficient splenic DCs was at least partly dependent on IL-6, but not TGFβ (21). Here, we find that LPS-stimulated LKB1-deficient GMDCs express significantly enhanced levels of IL-6, pro-IL-1β and IL-23p19, while TGFβ production was not affected. In addition, LKB1-deficient hepatic cDC2s express increased levels of *Il6* and *Il1b*, whereas *Tgfb1* was unchanged and *Il23a* undetectable. These data indicate that LKB1-deficient hepatic cDC2s display a cytokine profile that favors the development of pathogenic Th17 cells.

Recent single cell transcriptomics analysis of hepatic Th17 cells from HFD-fed obese mice identified two subsets, of which one was enriched during obesity. The accumulation of this inflammatory hepatic Th17 (ihTh17) subset was regulated through a CXCL9/10-CXCR3 axis, and these cells were sufficient to exacerbate NAFLD pathogenesis through glycolysis-facilitated production of proinflammatory cytokines IL-17A, TNF and IFNγ (16). Moreover, increased IL-6, TGFβ, IL-1β and IL-23 levels in steatotic livers were also reported in this study, suggesting involvement of DCs in generating these ihTh17 cells. Given their role in promoting NAFLD pathogenesis, it is tempting to speculate that LKB1-

deficient hepatic DCs promote accrual of these ihTh17 cells.

Deletion of AMPKα1 in DCs did not recapitulate the immunometabolic phenotype of CD11c[ΔLKB1] obese mice. Indeed, we and others have recently shown that LKB1 functions independently of AMPK in governing Tregs and Th17 cell differentiation (21, 22), which corresponds with a growing line of research showing AMPK-independent effects of LKB1 in immune cells (41, 55). We rather show that SIK inhibition, but not of the other DC-expressed AMPK-related kinases, increased expression of IL-6, IL-1β and IL-23 in GMDCs, indicating that an LKB1-SIK axis is likely involved in controlling the expression of cytokines that polarize pathogenic Th17 cells. The SIK family consists of three isoforms, SIK1-3, and is involved in regulating hepatic gluconeogenesis, lipid metabolism and tumorigenesis (56), although its underlying mechanisms are only beginning to be understood. SIKs control the phosphorylation and nucleocytoplasmic transport of class IIa histone deacetylases (HDACs) and cAMP-regulated transcriptional coactivators (CRTCs), identifying a role for SIKs in transcriptional regulation (57). CRTC is a coactivator of cAMP response element-binding protein (CREB) (58), and the promotors of *Il6*, *Il1b* and *Il23a* all contain CREB binding sites (59-61). It is thus tempting to speculate that inhibition of SIKs may promote CRTC nuclear transport, thereby promoting transcription of Th17-polarizing cytokines. In support of this, SIK1 and SIK3 were shown to control IL-6 production in tumor cells (62), and IL-6 and IL-1β production in Raw264.7 macrophages (63). Conversely, pharmacological inhibition of SIKs was also reported to suppress proinflammatory cytokines production in DCs and macrophages (64, 65). As SIK family members display functional redundancy in some settings (57), future studies are required to identify which SIK family member(s) control expression of Th17-polarizing cytokines, and what the mechanistic underpinnings are.

Among the limitations of our study, we cannot formally rule out that deletion of LKB1 in other CD11c-expressing cells, such as macrophages, contributed to the immunometabolic phenotype. Indeed, LysM[cre]-driven LKB1 deletion in macrophages increased LPS-induced proinflammatory cytokine production (41). However, these LysM[ΔLKB1] mice have unchanged Treg numbers (20), indicating that LKB1 deletion from macrophages does not alter T cell polarization *in vivo*. In addition, only partial knockout of *Stk11* was observed in macrophages from CD11c[ΔLKB1] mice (21, 66), which is likely attributable to lower CD11c expression by macrophages as compared to DCs. Furthermore, we found that expression of the proinflammatory/metaflammation-associated markers CD86 and CD11c on both eWAT and liver macrophages was either decreased or unchanged, as was *ex vivo* LPS-induced TNF production by macrophages from CD11c[ΔLKB1] mice (data not shown). Together, this makes it unlikely that macrophages play a dominant role in the immunometabolic phenotype of CD11c[ΔLKB1] mice.

Altogether, our data reveal a key role for LKB1 signaling in liver-resident DCs in limiting liver-specific and whole-body metabolic dysfunctions in the context of obesity, by

constraining hepatic Th17 accrual. We suggest the involvement of an LKB1-SIK axis to control expression of Th17-polarizing cytokines in DCs, opening interesting therapeutic options in controlling pathogenic Th17 cell development in metaflammation and other hyperinflammatory disorders.

Methods

Animals, diet and treatment

All experiments were performed in accordance with the Guide for the Care and Use of Laboratory Animals of the Institute for Laboratory Animal Research and have received approval from the Dutch Central Authority for Scientific Procedures on Animals (CCD; animal license number AVD116002015253). *Itgax*[cre] (CD11c; PMID: 17591855), *Stk11*^{fl/fl} (LKB1; PMID: 12226664), *Prkaa1*^{fl/fl} (AMPKα1; PMID: 21124450) and WT mice, all on C57Bl/6J background, were purchased from The Jackson Laboratory or Envigo and crossed, housed and bred at the LUMC. Mice were housed in a temperature-controlled room with a 12-hour light-dark cycle and ad libitum access to food and tap water under specific pathogen free conditions. To reduce variation due to sex hormone cycles on whole-body metabolism, male mice were used for all in vivo experiments. An a priori power calculation was done. Analysis was performed blinded to the conditions.

8-16 weeks old age-matched WT, *Stk11*^{fl/fl} (CD11c[WT]), *Itgax*[cre] *Stk11*^{fl/fl} (CD11c[ΔLKB1]), *Prkaa1*^{fl/fl} (CD11c[WT]) and *Itgax*[cre] *Prkaa1*^{fl/fl} (CD11c[ΔAMPKα1]) male mice were fed a high fat diet (HFD, 45% energy derived from fat, D12451, Research Diets) for 18-24 weeks as indicated.

For IL-17A neutralization experiments, 12-19 weeks old age-matched CD11c[WT] and CD11c[ΔLKB1] mice were systematically randomized over treatment groups based on body weight and fasting blood glucose levels, and fed a HFD for 6 weeks while concomitant biweekly treatment with 200 μg anti-mouse IL-17A (clone 17F3) or IgG1 κ isotype control (clone MOPC-21; both Bio X Cell). At sacrifice, spleen, visceral white adipose tissue (epididymal; eWAT), brown adipose tissue (intrascapular; BAT) and liver were weighed and collected for further processing.

Body composition and indirect calorimetry

Body composition was measured by MRI using an EchoMRI (Echo Medical Systems). Indirect calorimetry was performed in groups of 7-8 mice using a Comprehensive Laboratory Animal Monitoring System (Columbus Instruments) with free access to food and tap water.

Mice were individually housed at room temperature and a standard 12-hour light/dark cycle was maintained throughout the measurements. Mice were acclimated to the cages for a period of 48 hours before the start of 4 days of measurements at 20-minute intervals. Food intake was assessed by real-time feed weight measurements. Oxygen consumption and carbon dioxide production were measured, and based on this respirometry, energy expenditure (EE), and carbohydrate (CHO) and fatty acid (FA) oxidation were calculated as previously described (26).

Isolation of leukocytes from spleen

Spleens were collected in 500 μL RPMI 1640 + Glutamax (Life Technologies), mechanically disrupted, and digested for 20 min at 37 °C in medium supplemented with 1 mg/mL Collagenase D (Roche) and 2000 U/mL DNase I (Sigma-Aldrich). Digested samples were filtered through 100 μm filters and subjected to erythrocyte lysis buffer (0.15 M NH_4Cl, 1 mM $KHCO_3$, 0.1 mM Na_2EDTA) before counting using a hemocytometer.

Isolation of stromal vascular fraction from adipose tissue

After a 1-minute transcardial perfusion with PBS post sacrifice, eWAT samples were collected and digested as described previously (27, 28). In short, eWAT samples were minced and incubated for 1 hour at 37°C in an incubator under agitation (60 rpm) in HEPES-buffered Krebs solution, containing 0.5-1 g/L collagenase type I from *Clostridium histolyticum* (Sigma-Aldrich), 2% (w/v) dialyzed bovine serum albumin (BSA, fraction V; Sigma-Aldrich) and 6 mM D-Glucose (Sigma-Aldrich). The samples were passed through a 100 μm filter (Corning Life Sciences) which was washed with PBS supplemented with 2.5 mM EDTA and 5% FCS. After allowing the adipocytes to settle for ~10 min, the infranatant, consisting of immune cells, was collected and pelleted at 350 x g for 10 min at room temperature. The pellet was treated with erythrocyte lysis buffer, washed with PBS/EDTA/FCS, and counted using a hemocytometer.

Isolation of leukocytes from liver

Livers were collected and digested as described previously (27, 28). In short, livers were minced and incubated for 45 min at 37°C in RPMI 1640 + Glutamax containing 1 mg/mL collagenase type IV from *Clostridium histolyticum*, 200 U/mL DNase (both Sigma-Aldrich) and 1 mM $CaCl_2$. The digested tissues were passed through a 100 μm cell strainer (Corning Life Sciences) which was subsequently washed with PBS/EDTA/FCS. After

centrifugation (530 x g, 10 min at 4°C), cells were resuspended in 30 mL PBS/EDTA/FCS and spun down at 50 x g for 3 min at 4°C to pellet the hepatocytes. The supernatant was collected, treated with erythrocyte lysis buffer and CD45$^+$ leukocytes were isolated using LS columns and CD45 MicroBeads (35 μL beads per sample, Miltenyi Biotec) according to the manufacturer's protocol. Isolated liver leukocytes were counted using a hemocytometer.

Flow cytometry

For assessing LKB1/ACC phosphorylation state in spleen, eWAT and liver, tissues were collected and immediately minced in 1.85% formaldehyde solution (Sigma-Aldrich) and digested as described above. Isolated cell suspensions were permanently permeabilized using 100% methanol for 10 min at -20°C. For other purposes, spleen, eWAT and liver cell suspensions were stained using a Fixable Aqua Dead Cell Stain Kit (Invitrogen) or Zombie UV Fixable Viability Kit (Biolegend) for 20 min at room temperature. Unless sorted or measured alive, cells were fixed for 1 h at 4°C using a FOXP3/Transcription Factor Staining Buffer Set (Invitrogen, for FOXP3 detection) or 15 min at room temperature using a 1.85% formaldehyde solution in PBS (Sigma-Aldrich, for everything else). For detection of intracellular cytokines, isolated cells were cultured for 4 h in RPMI 1640 + Glutamax in the presence of 100 ng/mL phorbol myristate acetate (PMA), 1 μg/mL ionomycin, 10 μg/mL Brefeldin A (all from Sigma-Aldrich). After 4 hours, cells were washed with PBS, stained with Aqua, and fixed as described above. Cell suspensions were first pre-incubated with 2.4G2 antibody (kindly provided by Louis Boon) for blocking Fc receptors and next stained for surface markers in PBS supplemented with 0.5% BSA (Roche) and 2 mM EDTA (Sigma-Aldrich) and antibodies for 30 min at 4°C. For detection of phosphorylated proteins, FOXP3 and intracellular cytokines, cell suspensions were stained in Permeabilization Buffer (eBioscience) instead. Phosphorylated Ser79-ACC and Ser431-LKB1 were stained using unconjugated rabbit-anti-mouse antibodies prior to staining with other antibodies and goat-anti-rabbit-Alexa Fluor 647. Antibody information is provided in Supplementary Table 1 and gating strategies shown in Supplementary Figure 1. Cells were measured on a FACSCanto II or LSR II and analyzed using FlowJo (Version 10.6, TreeStar).

Plasma analysis

Blood samples were collected from the tail tip of 4 h-fasted mice using paraoxon-coated glass capillaries. Fasting blood glucose level was determined using a hand-held Glucometer (Accu-Check; Roche Diagnostics) and plasma insulin level was measured using a commercial kit as per manufacturer's instructions (Chrystal Chem).

Insulin- and glucose tolerance tests

Whole-body insulin tolerance test (ipITT) and glucose tolerance test (ipGTT) were performed 1 week before sacrifice, as previously described (27, 28). In short, a bolus of insulin (0.75U/kg body mass, NOVORAPID, Novo Nordisk) was administered intraperitoneally (i.p.) to 4 h-fasted mice, after which blood glucose levels were measured at t=0, 15, 30, 45 and 60 min post insulin administration using a Glucometer. For ipGTT, 6 h-fasted mice were injected i.p. with 2g/kg total body mass of D-Glucose (Sigma-Aldrich) and blood glucose was measured at t=0, 20, 40, 60 and 90 min post glucose injection using a Glucometer.

Histological analysis

Pieces of eWAT and liver (~30 mg) were fixed in 4% formaldehyde solution (Sigma-Aldrich), paraffin-embedded, sectioned at 4 µm and stained with Hematoxylin and Eosin (H&E). Six fields at 20x magnification (total area 1.68 mm^2) were used for the analysis of adipocyte size, crown-like structures or hepatic steatosis.

Hepatic lipid composition

Liver lipids were extracted as previously described (29). Liver triglyceride and total cholesterol concentrations were measured using commercial kits (all from Instruchemie) and expressed as nanomoles per milligram of total protein content using the Bradford protein assay kit (Sigma-Aldrich).

In vivo DC expansion, isolation and sorting

To expand the DC pool *in vivo*, 2×10^6 Flt3L-secreting B16 melanoma cells (kind gift from Dr. Edward Pearce) in 100 µL HBSS were injected subcutaneously into the flank of mice. After 10 days, spleen, liver and eWAT were harvested, and digested and processed as described earlier. cDC2s were further enriched from single cell suspensions by positive isolation with CD11c Microbeads (Miltenyi Biotec; per manufacturer's instructions) and FACS sorting (MHCII^{+} CD11c^{+} CD64^{-} F4/80^{-} CD172a^{+} XCR1^{-}) on a BD FACSAria using a 100 µm nozzle at 20 PSI. Subsequently, sorted cDC2s were stimulated with 100 ng/mL LPS for 16 h for assessing cytokine expression by RT-qPCR.

BM-derived DC cultures

Bone marrow-derived DCs were cultured as described previously (22). Briefly, bone marrow cells were flushed from femurs and tibias, and 5×10^6 cells were plated in tissue culture-

treated petri dishes (NUNC) in 10 mL of differentiation medium, consisting of RMPI 1640 Glutamax (Gibco) supplemented with 5% FCS (Gibco), 25 nM β-mercaptoethanol (Sigma-Aldrich), 100 U/mL penicillin, 100 µg/mL streptomycin and 20 ng/mL of murine GM-CSF (PeproTech). Medium was refreshed on day 4 and day 7, after which on day 9 non-adherent GMDCs were harvested. 1×10^5 GMDCs were seeded in a round-bottom 96-well plate and rested overnight. The next day, GMDCs were incubated for 2 h at 37°C with 50 µM MARK inhibitor (MARK/Par-1 Activity Inhibitor, 39621; Calbiochem), 50 nM SIK inhibitor (HG-9-91-01; Cayman Chemical), 1 µM NUAK inhibitor (WZ 4003; Tocris) or 5 µM AMPK inhibitor (SBI-0206965; Sigma-Aldrich). After 2 h, LPS and Brefeldin A were added to a final concentration of 100 ng/mL and 10 µg/mL, respectively, and samples were incubated for an additional 4 h at 37°C. After 6 h, cells were stained with a viability kit, fixed using 1.85% formaldehyde and stored at 4°C until further processing for intracellular cytokine detection by flow cytometry.

RNA-isolation and RT-qPCR

RNA was extracted from LPS-stimulated sorted cDC2s or GMDCs using TriPure RNA Isolation reagent. Total RNA (200-400 ng) was reverse transcribed using the M-MLV Reverse Transcriptase kit (ThermoFisher). Real-time qPCR runs were performed on a CFX96 Real-time C1000 thermal cycler (Biorad) using the GoTaq qPCR Master Mix kit (Promega). Gene expression was normalized to the housekeeping gene *Rplp0* and expressed as fold change compared to CD11c^{WT} samples. A list of primer sequences can be found in Supplementary Table 2.

Statistical analysis

All data are presented as mean ± standard error of the mean (SEM). Statistical analysis was performed using GraphPad Prism version 8 for Windows (GraphPad Software) with unpaired t-test, one-way or two-way analysis of variance (ANOVA) followed by Fisher's post-hoc test. Differences between groups were considered statistically significant at P < 0.05.

Acknowledgements

5

References

1.	Gregor MF, Hotamisligil GS. Inflammatory mechanisms in obesity. Annu Rev Immunol. 2011;29:415-45.

2.	van der Zande HJP, Zawistowska-Deniziak A, Guigas B. Immune Regulation of Metabolic Homeostasis by Helminths and Their Molecules. Trends Parasitol. 2019;35(10):795-808.

3.	Hotamisligil GS, Shargill NS, Spiegelman BM. Adipose expression of tumor necrosis factor-alpha: direct role in obesity-linked insulin resistance. Science. 1993;259(5091):87-91.

4.	Stienstra R, Joosten LA, Koenen T, van Tits B, van Diepen JA, van den Berg SA, et al. The inflammasome-mediated caspase-1 activation controls adipocyte differentiation and insulin sensitivity. Cell Metab. 2010;12(6):593-605.

5.	Bertola A, Ciucci T, Rousseau D, Bourlier V, Duffaut C, Bonnafous S, et al. Identification of adipose tissue dendritic cells correlated with obesity-associated insulin-resistance and inducing Th17 responses in mice and patients. Diabetes. 2012;61(9):2238-47.

6.	Stefanovic-Racic M, Yang X, Turner MS, Mantell BS, Stolz DB, Sumpter TL, et al. Dendritic cells promote macrophage infiltration and comprise a substantial proportion of obesity-associated increases in CD11c+ cells in adipose tissue and liver. Diabetes. 2012;61(9):2330-9.

7.	Cho KW, Zamarron BF, Muir LA, Singer K, Porsche CE, DelProposto JB, et al. Adipose Tissue Dendritic Cells Are Independent Contributors to Obesity-Induced Inflammation and Insulin Resistance. J Immunol. 2016;197(9):3650-61.

8.	Deczkowska A, David E, Ramadori P, Pfister D, Safran M, At The B, et al. XCR1(+) type 1 conventional dendritic cells drive liver pathology in non-alcoholic steatohepatitis. Nat Med. 2021;27(6):1043-54.

9.	Wu D, Molofsky AB, Liang HE, Ricardo-Gonzalez RR, Jouihan HA, Bando JK, et al. Eosinophils sustain adipose alternatively activated macrophages associated with glucose homeostasis. Science. 2011;332(6026):243-7.

10.	Molofsky AB, Nussbaum JC, Liang HE, Van Dyken SJ, Cheng LE, Mohapatra A, et al. Innate lymphoid type 2 cells sustain visceral adipose tissue eosinophils and alternatively activated macrophages. J Exp Med. 2013;210(3):535-49.

11.	Feuerer M, Herrero L, Cipolletta D, Naaz A, Wong J, Nayer A, et al. Lean, but not obese, fat is enriched for a unique population of regulatory T cells that affect metabolic parameters. Nat Med. 2009;15(8):930-9.

12.	Tang Y, Bian Z, Zhao L, Liu Y, Liang S, Wang Q, et al. Interleukin-17 exacerbates hepatic steatosis and inflammation in non-alcoholic fatty liver disease. Clin Exp Immunol. 2011;166(2):281-90.

13.	Fabbrini E, Cella M, McCartney SA, Fuchs A, Abumrad NA, Pietka TA, et al. Association between specific adipose tissue CD4+ T-cell populations and insulin resistance in obese individuals. Gastroenterology. 2013;145(2):366-74 e1-3.

14.	Harley IT, Stankiewicz TE, Giles DA, Softic S, Flick LM, Cappelletti M, et al. IL-17 signaling accelerates the progression of nonalcoholic fatty liver disease in mice. Hepatology. 2014;59(5):1830-9.

15. Gomes AL, Teijeiro A, Buren S, Tummala KS, Yilmaz M, Waisman A, et al. Metabolic Inflammation-Associated IL-17A Causes Non-alcoholic Steatohepatitis and Hepatocellular Carcinoma. Cancer Cell. 2016;30(1):161-75.

16. Moreno-Fernandez ME, Giles DA, Oates JR, Chan CC, Damen M, Doll JR, et al. PKM2-dependent metabolic skewing of hepatic Th17 cells regulates pathogenesis of non-alcoholic fatty liver disease. Cell Metab. 2021;33(6):1187-204 e9.

17. Patente TA, Pelgrom LR, Everts B. Dendritic cells are what they eat: how their metabolism shapes T helper cell polarization. Curr Opin Immunol. 2019;58:16-23.

18. Pearce EJ, Everts B. Dendritic cell metabolism. Nat Rev Immunol. 2015;15(1):18-29.

19. Brombacher EC, Everts B. Shaping of Dendritic Cell Function by the Metabolic Micro-Environment. Front Endocrinol (Lausanne). 2020;11:555.

20. Chen S, Fang L, Guo W, Zhou Y, Yu G, Li W, et al. Control of Treg cell homeostasis and immune equilibrium by Lkb1 in dendritic cells. Nat Commun. 2018;9(1):5298.

21. Wang Y, Du X, Wei J, Long L, Tan H, Guy C, et al. LKB1 orchestrates dendritic cell metabolic quiescence and anti-tumor immunity. Cell Res. 2019;29(5):391-405.

22. Pelgrom LR, Patente TA, Sergushichev A, Esaulova E, Otto F, Ozir-Fazalalikhan A, et al. LKB1 expressed in dendritic cells governs the development and expansion of thymus-derived regulatory T cells. Cell Res. 2019;29(5):406-19.

23. Jaleel M, McBride A, Lizcano JM, Deak M, Toth R, Morrice NA, et al. Identification of the sucrose non-fermenting related kinase SNRK, as a novel LKB1 substrate. FEBS Lett. 2005;579(6):1417-23.

24. Lizcano JM, Goransson O, Toth R, Deak M, Morrice NA, Boudeau J, et al. LKB1 is a master kinase that activates 13 kinases of the AMPK subfamily, including MARK/PAR-1. EMBO J. 2004;23(4):833-43.

25. Shackelford DB, Shaw RJ. The LKB1-AMPK pathway: metabolism and growth control in tumour suppression. Nat Rev Cancer. 2009;9(8):563-75.

26. van der Zande HJP, Lambooij JM, Chavanelle V, Zawistowska-Deniziak A, Otero Y, Otto F, et al. Effects of a novel polyphenol-rich plant extract on body composition, inflammation, insulin sensitivity, and glucose homeostasis in obese mice. Int J Obes (Lond). 2021.

27. Hussaarts L, Garcia-Tardon N, van Beek L, Heemskerk MM, Haeberlein S, van der Zon GC, et al. Chronic helminth infection and helminth-derived egg antigens promote adipose tissue M2 macrophages and improve insulin sensitivity in obese mice. FASEB J. 2015;29(7):3027-39.

28. van der Zande HJP, Gonzalez MA, de Ruiter K, Wilbers RHP, Garcia-Tardon N, van Huizen M, et al. The helminth glycoprotein omega-1 improves metabolic homeostasis in obese mice through type 2 immunity-independent inhibition of food intake. FASEB J. 2021;35(2):e21331.

29. Thomas A, Belaidi E, Moulin S, Horman S, van der Zon GC, Viollet B, et al. Chronic Intermittent Hypoxia Impairs Insulin Sensitivity but Improves Whole-Body Glucose Tolerance by Activating Skeletal Muscle AMPK. Diabetes. 2017;66(12):2942-51.

30. Teijeiro A, Garrido A, Ferre A, Perna C, Djouder N. Inhibition of the IL-17A axis in adipocytes suppresses diet-induced obesity and metabolic disorders in mice. Nat Metab. 2021;3(4):496-512.

5

31. Nishimura T, Saito Y, Washio K, Komori S, Respatika D, Kotani T, et al. SIRPalpha on CD11c(+) cells induces Th17 cell differentiation and subsequent inflammation in the CNS in experimental autoimmune encephalomyelitis. Eur J Immunol. 2020;50(10):1560-70.

32. Nieves W, Hung LY, Oniskey TK, Boon L, Foretz M, Viollet B, et al. Myeloid-Restricted AMPKalpha1 Promotes Host Immunity and Protects against IL-12/23p40-Dependent Lung Injury during Hookworm Infection. J Immunol. 2016;196(11):4632-40.

33. Xie Z, Dong Y, Scholz R, Neumann D, Zou MH. Phosphorylation of LKB1 at serine 428 by protein kinase C-zeta is required for metformin-enhanced activation of the AMP-activated protein kinase in endothelial cells. Circulation. 2008;117(7):952-62.

34. Sapkota GP, Kieloch A, Lizcano JM, Lain S, Arthur JS, Williams MR, et al. Phosphorylation of the protein kinase mutated in Peutz-Jeghers cancer syndrome, LKB1/STK11, at Ser431 by p90(RSK) and cAMP-dependent protein kinase, but not its farnesylation at Cys(433), is essential for LKB1 to suppress cell vrowth. J Biol Chem. 2001;276(22):19469-82.

35. Houde Vanessa P, Ritorto Maria S, Gourlay R, Varghese J, Davies P, Shpiro N, et al. Investigation of LKB1 Ser431 phosphorylation and Cys433 farnesylation using mouse knockin analysis reveals an unexpected role of prenylation in regulating AMPK activity. Biochemical Journal. 2014;458(1):41-56.

36. Song P, Xie Z, Wu Y, Xu J, Dong Y, Zou MH. Protein kinase Czeta-dependent LKB1 serine 428 phosphorylation increases LKB1 nucleus export and apoptosis in endothelial cells. J Biol Chem. 2008;283(18):12446-55.

37. Nagpal R, Newman TM, Wang S, Jain S, Lovato JF, Yadav H. Obesity-Linked Gut Microbiome Dysbiosis Associated with Derangements in Gut Permeability and Intestinal Cellular Homeostasis Independent of Diet. J Diabetes Res. 2018;2018:3462092.

38. Thaiss CA, Itav S, Rothschild D, Meijer MT, Levy M, Moresi C, et al. Persistent microbiome alterations modulate the rate of post-dieting weight regain. Nature. 2016;540(7634):544-51.

39. Liu R, Hong J, Xu X, Feng Q, Zhang D, Gu Y, et al. Gut microbiome and serum metabolome alterations in obesity and after weight-loss intervention. Nat Med. 2017;23(7):859-68.

40. Martin-Mateos R, Albillos A. The Role of the Gut-Liver Axis in Metabolic Dysfunction-Associated Fatty Liver Disease. Front Immunol. 2021;12:660179.

41. Liu Z, Zhang W, Zhang M, Zhu H, Moriasi C, Zou MH. Liver kinase B1 suppresses lipopolysaccharide-induced nuclear factor kappaB (NF-kappaB) activation in macrophages. J Biol Chem. 2015;290(4):2312-20.

42. Zhao ZH, Wang ZX, Zhou D, Han Y, Ma F, Hu Z, et al. Sodium Butyrate Supplementation Inhibits Hepatic Steatosis by Stimulating Liver Kinase B1 and Insulin-Induced Gene. Cell Mol Gastroenterol Hepatol. 2021.

43. Li C, Wang G, Sivasami P, Ramirez RN, Zhang Y, Benoist C, et al. Interferon-alpha-producing plasmacytoid dendritic cells drive the loss of adipose tissue regulatory T cells during obesity. Cell Metab. 2021.

44. Han JM, Wu D, Denroche HC, Yao Y, Verchere CB, Levings MK. IL-33 Reverses an Obesity-Induced Deficit in Visceral Adipose Tissue ST2+ T Regulatory Cells and Ameliorates Adipose Tissue Inflammation and Insulin Resistance. J Immunol. 2015;194(10):4777-83.

45. Wara AK, Wang S, Wu C, Fang F, Haemmig S, Weber BN, et al. KLF10 Deficiency in CD4(+) T Cells Triggers Obesity, Insulin Resistance, and Fatty Liver. Cell Rep. 2020;33(13):108550.

46. Bapat SP, Myoung Suh J, Fang S, Liu S, Zhang Y, Cheng A, et al. Depletion of fat-resident Treg cells prevents age-associated insulin resistance. Nature. 2015;528(7580):137-41.

47. Wu D, Wong CK, Han JM, Orban PC, Huang Q, Gillies J, et al. T reg-specific insulin receptor deletion prevents diet-induced and age-associated metabolic syndrome. J Exp Med. 2020;217(8).

48. Beppu LY, Mooli RGR, Qu X, Marrero GJ, Finley CA, Fooks AN, et al. Tregs facilitate obesity and insulin resistance via a Blimp-1/IL-10 axis. JCI Insight. 2021;6(3).

49. Ma X, Hua J, Mohamood AR, Hamad ARA, Ravi R, Li Z. A high-fat diet and regulatory T cells influence susceptibility to endotoxin-induced liver injury. Hepatology. 2007;46(5):1519-29.

50. Volpe E, Servant N, Zollinger R, Bogiatzi SI, Hupe P, Barillot E, et al. A critical function for transforming growth factor-beta, interleukin 23 and proinflammatory cytokines in driving and modulating human T(H)-17 responses. Nat Immunol. 2008;9(6):650-7.

51. Manel N, Unutmaz D, Littman DR. The differentiation of human T(H)17 cells requires transforming growth factor-beta and induction of the nuclear receptor RORgammat. Nat Immunol. 2008;9(6):641-9.

52. Ghoreschi K, Laurence A, Yang XP, Tato CM, McGeachy MJ, Konkel JE, et al. Generation of pathogenic T(H)17 cells in the absence of TGF-beta signalling. Nature. 2010;467(7318):967-71.

53. Lee Y, Awasthi A, Yosef N, Quintana FJ, Xiao S, Peters A, et al. Induction and molecular signature of pathogenic TH17 cells. Nat Immunol. 2012;13(10):991-9.

54. Scott CL, Tfp ZM, Beckham KS, Douce G, Mowat AM. Signal regulatory protein alpha (SIRPalpha) regulates the homeostasis of CD103(+) CD11b(+) DCs in the intestinal lamina propria. Eur J Immunol. 2014;44(12):3658-68.

55. He N, Fan W, Henriquez B, Yu RT, Atkins AR, Liddle C, et al. Metabolic control of regulatory T cell (Treg) survival and function by Lkb1. Proc Natl Acad Sci U S A. 2017;114(47):12542-7.

56. Sun Z, Jiang Q, Li J, Guo J. The potent roles of salt-inducible kinases (SIKs) in metabolic homeostasis and tumorigenesis. Signal Transduct Target Ther. 2020;5(1):150.

57. Wein MN, Foretz M, Fisher DE, Xavier RJ, Kronenberg HM. Salt-Inducible Kinases: Physiology, Regulation by cAMP, and Therapeutic Potential. Trends Endocrinol Metab. 2018;29(10):723-35.

58. Altarejos JY, Montminy M. CREB and the CRTC co-activators: sensors for hormonal and metabolic signals. Nat Rev Mol Cell Biol. 2011;12(3):141-51.

59. Dendorfer U, Oettgen P, Libermann TA. Multiple regulatory elements in the interleukin-6 gene mediate induction by prostaglandins, cyclic AMP, and lipopolysaccharide. Mol Cell Biol. 1994;14(7):4443-54.

60. Chandra G, Cogswell JP, Miller LR, Godlevski MM, Stinnett SW, Noel SL, et al. Cyclic AMP signaling pathways are important in IL-1 beta transcriptional regulation. J Immunol. 1995;155(10):4535-43.

5

61.   Kocieda VP, Adhikary S, Emig F, Yen JH, Toscano MG, Ganea D. Prostaglandin E2-induced IL-23p19 subunit is regulated by cAMP-responsive element-binding protein and C/AATT enhancer-binding protein beta in bone marrow-derived dendritic cells. J Biol Chem. 2012;287(44):36922-35.

62.   Hollstein PE, Eichner LJ, Brun SN, Kamireddy A, Svensson RU, Vera LI, et al. The AMPK-Related Kinases SIK1 and SIK3 Mediate Key Tumor-Suppressive Effects of LKB1 in NSCLC. Cancer Discov. 2019;9(11):1606-27.

63.   Yong Kim S, Jeong S, Chah KH, Jung E, Baek KH, Kim ST, et al. Salt-inducible kinases 1 and 3 negatively regulate Toll-like receptor 4-mediated signal. Mol Endocrinol. 2013;27(11):1958-68.

64.   Lombardi MS, Gillieron C, Dietrich D, Gabay C. SIK inhibition in human myeloid cells modulates TLR and IL-1R signaling and induces an anti-inflammatory phenotype. J Leukoc Biol. 2016;99(5):711-21.

65.   Sundberg TB, Choi HG, Song JH, Russell CN, Hussain MM, Graham DB, et al. Small-molecule screening identifies inhibition of salt-inducible kinases as a therapeutic strategy to enhance immunoregulatory functions of dendritic cells. Proc Natl Acad Sci U S A. 2014;111(34):12468-73.

66.   Caton ML, Smith-Raska MR, Reizis B. Notch-RBP-J signaling controls the homeostasis of CD8- dendritic cells in the spleen. J Exp Med. 2007;204(7):1653-64.

Supplementary information

Supplementary Table 1. Antibodies and reagents for flow cytometry

Target	Clone	Conjugate	Source	Identifier
B220	RA3-6B2	FITC	eBioscience	11-0452
CD3	17A2	APC-eF780	eBioscience	47-0032
CD3	17A2	BV605	Biolegend	100237
CD3	17A2	FITC	eBioscience	11-0032
CD4	GK1.5	BV650	BD Biosciences	563232
CD4	GK1.5	PE-Cy7	eBioscience	25-0041
CD4	GK1.5	PerCP-eFluor 710	eBioscience	46-0041
CD8a	53-6.7	BV711	Biolegend	100759
CD8a	53-6.7	PE	eBioscience	12-0081
CD11b	M1/70	FITC	eBioscience	11-0112
CD11b	M1/70	PE-Cy7	eBioscience	25-0112
CD11c	N418	BV421	Biolegend	117330
CD11c	HL3	FITC	BD Biosciences	553801
CD11c	HL3	Horizon V450	BD Biosciences	560521
CD11c	N418	PE-Cy7	eBioscience	25-0114
CD19	MB19-1	FITC	eBioscience	11-0191
CD40	HM40-3	FITC	eBioscience	11-0402
CD44	IM7	eFluor 450	eBioscience	48-0441
CD45	30-F11	BV785	Biolegend	103149
CD45.2	104	FITC	Biolegend	109806
CD45.2	104	eFluor 450	eBioscience	48-0454
CD64	X54-5/7.1	PE	Biolegend	139304
CD64	X54-5/7.1	PE/Dazzle 594	Biolegend	139319
CD64	X54-5/7.1	PerCP-Cy5.5	Biolegend	139308
CD80	16-10A1	APC	eBioscience	17-0801
CD86	GL-1	APC/Fire 750	Biolegend	105045
CD86	GL-1	PE	BD Biosciences	553692
CD172a	P84	PE	Biolegend	144011
CD197/CCR7	4B12	PerCP-Cy5.5	Biolegend	120116
F4/80	BM8	APC	eBioscience	17-4801
F4/80	BM8	BV711	Biolegend	123147
FOXP3	FJK-16s	APC	eBioscience	17-5773
Goat-anti-Rabbit	Polyclonal	Alexa Fluor 647	Invitrogen	A21244
GR-1	RB6-8C5	FITC	BD Biosciences	553126
IFNγ	XMG1.2	FITC	eBioscience	11-7311
IL-5	TRFK5	PE	Biolegend	504303
IL-6	MP5-20F3	APC	Biolegend	504507
IL-17A	eBio17B7	PE-Cy7	eBioscience	25-7177
IL-17A	TC11-18H10.1	PerCP-Cy5.5	Biolegend	506919

5

Target	Clone	Conjugate	Source	Identifier
IL-23p19	fc23cpg	eFluor 660	Invitrogen	50-7023
LAP	TW7-16B4	PerCP-eF710	Invitrogen	46-9821
Ly6C	HK1.4	APC-Cy7	Biolegend	128026
MHCI/H-2Kb	AF6-88.5	Pacific Blue	Biolegend	116514
MHCII	M5/114 15.2	Alexa Fluor 700	Invitrogen	56-5321
MHCII	M5/114 15.2	APC-eFluor 780	eBioscience	47-5321
MHCII	M5/114 15.2	FITC	eBioscience	11-5321
NK1.1	PK136	FITC	eBioscience	11-5941
Phospho-ACC (Ser79)	D7D11	-	Cell Signaling	11818S
Phospho-LKB1 (Ser431)	C67A3	-	Cell Signaling	3482S
Pro-IL-1β	NJTEN3	PE	Invitrogen	12-7114
Siglec-F	E50-2440	PE	BD Biosciences	552126
XCR1	ZET	BV650	Biolegend	148220
Other reagents			**Source**	**Identifier**
LIVE/DEAD™ Fixable Aqua Dead Cell Stain Kit			Invitrogen	L34957
Zombie UV™ Fixable Viability Kit			Biolegend	423107

Supplementary Table 2. qPCR primers

| Gene	Accession number	Forward primer	Reverse primer
Il1b	NM_008361	GACCCCAAAAGATGAAGGGCT	ATGTGCTGCTGCGAGATTTG
Il6	NM_031168.2	CCTCTCTGCAAGAGACTTCCAT	ACAGGTCTGTTGGGAGTGGT
Il23a	NM_031252.2	GCACCAGCGGGACATATGAA	CAAGCAGAACTGGCTGTTGTC
Rplp0	NM_007475	TCTGGAGGGTGTCCGCAACG	GCCAGGACGCGCTTGTACCC
Stk11	NM_011492.4	GTGCCAAGCTCATGGGTACT	CACCGAGGTCGGAGATCTTG
Tgfb1	NM_011577	GCTGAACCAAGGAGACGGAA	ATGTCATGGATGGTGCCCAG
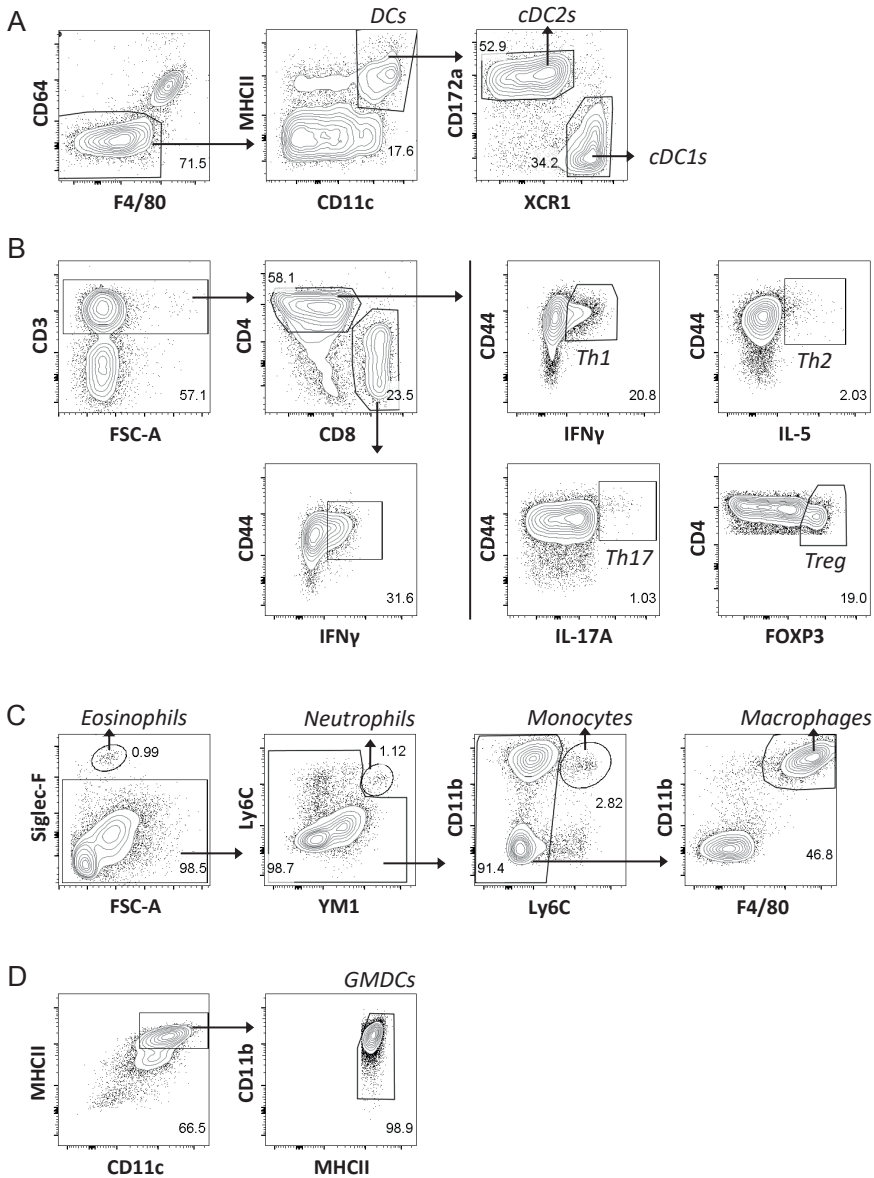
Supplementary Figure 1. Gating strategies. (**A**) Gating strategy for analysis of DCs and cDC subsets. CD11b and CD8a were used as alternatives for CD172a and XCR1, respectively. (**B**) Gating strategy for T (helper) cell subsets is shown. (**C**) Gating strategy for identification of myeloid cell subsets. (**D**) Gating strategy for identification of GMDCs. Isolated cells were pre-gated on live CD45+ single cells. For T (helper) cell subset analysis, cells were additionally pre-gated as lineage-, which included antibodies directed against B220, CD11b, CD11c, GR-1 and NK1.1. Representative sample was chosen from eWAT samples for A-C. Gating strategies were similar for the indicated cell populations in liver and spleen.
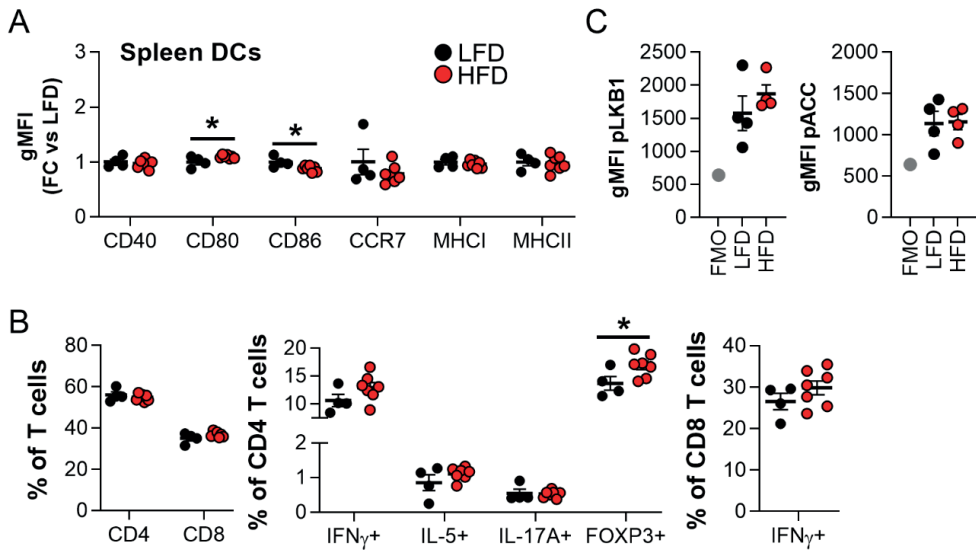
Supplementary Figure 2. Splenic DCs and T cells are mostly unaffected by obesity. Mice were fed a LFD (black symbols) or a HFD (red symbols) for 24 weeks. (**A**) At sacrifice, spleen was collected and immune cells were isolated and analyzed by flow cytometry. Relative expression of indicated DC markers by splenic DCs. (**B**) Cells were restimulated with PMA/ionomycin in the presence of Brefeldin A for detection of intracellular cytokines, and were analyzed by flow cytometry. CD4 and CD8 T cell, Th1, Th2, Th17 and Treg CD4 T cell, and IFNγ+ CD8 T cell percentages in spleen. (**C**) Spleens were immediately formaldehyde-fixed after collection and immune cells were isolated. Phosphorylated LKB1 (Ser431) and ACC (Ser79) were measured in DCs from spleen by flow cytometry. Results are expressed as means ± SEM. * $P<0.05$ vs LFD (n = 4-7 mice per group). Related to figure 1.
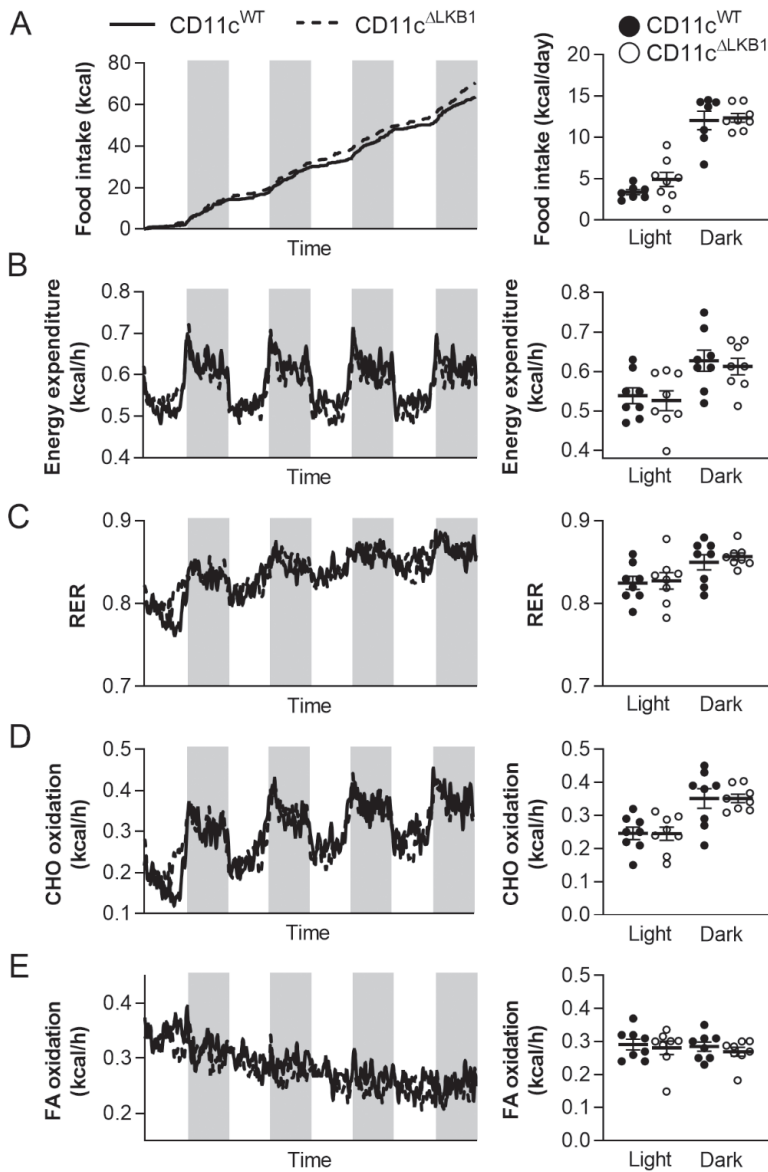
**Supplementary Figure 3. LKB1 deficiency in DCs did not affect food intake and whole-body energy expenditure.** CD11c^{WT} (black symbols) and CD11c$^{\Delta LKB1}$ (open symbols) mice were fed a HFD for 18 weeks. At week 15, mice were subjected to individual indirect calorimetric measurements using fully automated metabolic cages with free access to food and water. (**A-E**) Cumulative food intake (*A*), energy expenditure (EE; *B*), respiratory exchange rate (RER; *C*), carbohydrate (CHO; *D*) and fatty acid (FA; *E*) oxidation were measured for 4 consecutive days (white part = light phase; grey part = dark phase). The daily averages for each of the abovementioned parameters were calculated. Results are expressed as means ± SEM. (n = 7-8 mice per group). Related to figure 2.
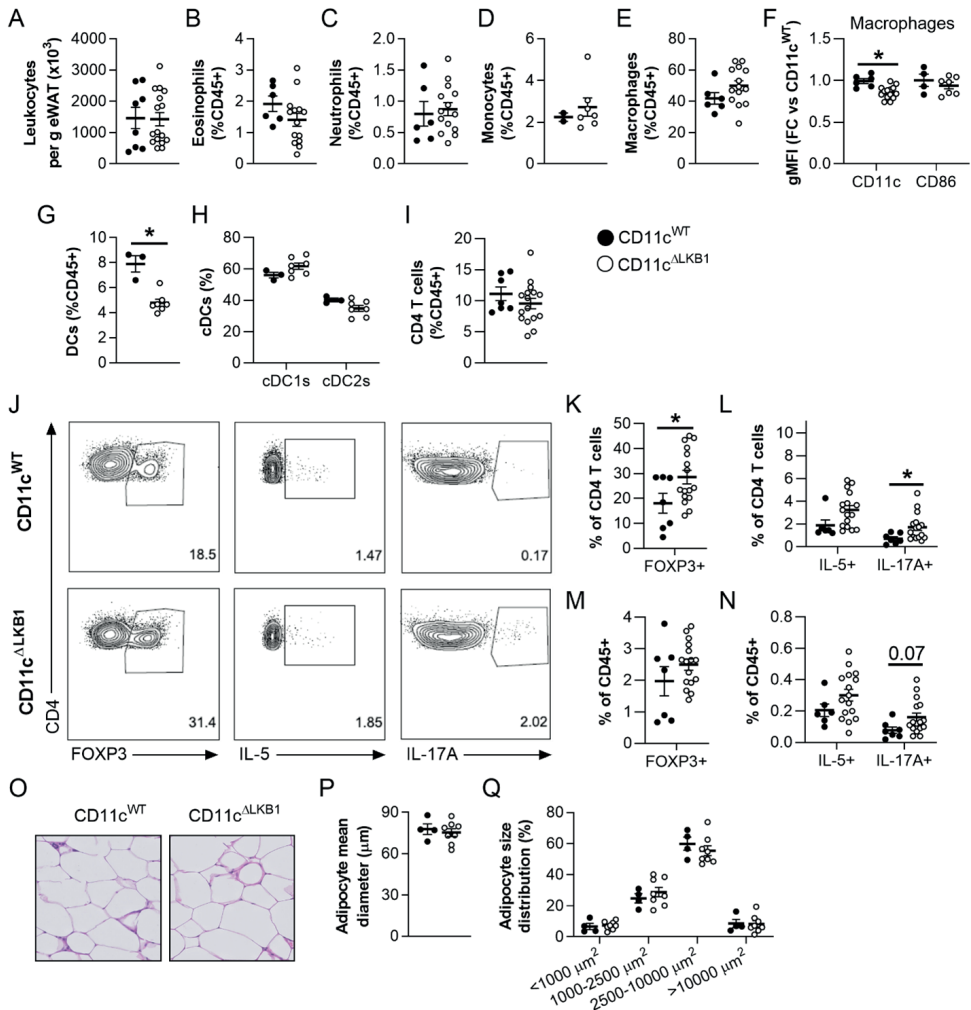
Supplementary Figure 4. LKB1 deficiency in DCs did not aggravate adipose tissue immunometabolic dysfunctions in obese mice. CD11c^{WT} (black symbols) and CD11c$^{\Delta LKB1}$ mice (open symbols) were fed a HFD for 18 weeks. (**A-I**) At sacrifice, eWAT was collected and immune cells isolated and analyzed by flow cytometry. Total leukocytes per gram eWAT were quantified (*A*). Percentages of eosinophils (*B*), neutrophils (*C*), monocytes (*D*) and macrophages (*E*) in eWAT expressed as frequencies of total leukocytes. Expression of CD11c and CD86 on eWAT macrophages relative to CD11c^{WT} mice (*F*). Abundances of DCs (*G*), cDC subsets (*H*) and CD4 T cells (*I*). (**J-N**) eWAT immune cells were restimulated with PMA and ionomycin in the presence of Brefeldin A for intracellular cytokine detection. Representative plots (*J*) and percentages of FOXP3$^+$ Treg (*K,M*), IL-5$^+$ Th2 and IL-17A$^+$ Th17 cells (*L,N*) were determined as frequencies of CD4 T cells (*K,L*) and total leukocytes (*M,N*). (**O**) A part of eWAT was sectioned and H&E-stained. (**P-Q**) Mean adipocyte diameter (*P*) and adipocyte size distribution (*Q*) were quantified from H&E stained slides. Data shown are a pool of two independent experiments, except for D, F-H and O-Q. Results are expressed as means ± SEM. * P<0.05 vs CD11c^{WT} (n = 7-16 mice per group for A-C, E and I-N; n = 3-8 mice per group for D, F-H and O-Q).
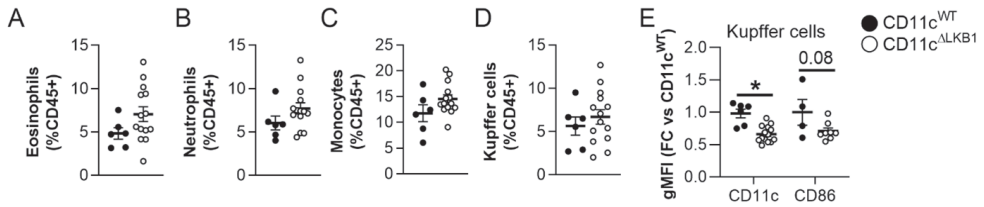
Supplementary Figure 5. Effects of LKB1 deletion from DCs on myeloid cell subsets in the liver. CD11c^{WT} (black symbols) and CD11c$^{\Delta LKB1}$ (open symbols) mice were fed a HFD for 18 weeks. At sacrifice, liver was collected and immune cells were isolated and analyzed by flow cytometry. (**A-E**) Percentages of hepatic eosinophils (*A*), neutrophils (*B*), monocytes (*C*) and Kupffer cells (*D*) expressed as frequencies of total leukocytes. Expression of CD11c and CD86 on Kupffer cells, expressed as fold change *vs* CD11c^{WT} (*E*). Data shown are a pool of two independent experiments, except for CD86 expression in E. Results are expressed as means ± SEM. * P<0.05 vs CD11c^{WT} (n = 4-14 mice per group). Related to figure 3.

5
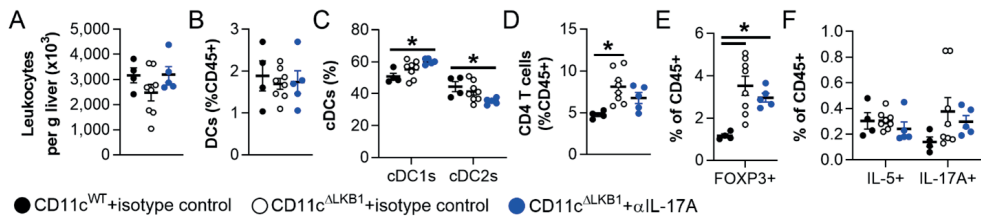
Supplementary Figure 6. Effects of IL-17A neutralization on hepatic immune cells. Mice were treated as described in the legend of figure 5. (**A-D**) At sacrifice, liver was collected and immune cells were isolated and phenotyped by flow cytometry. Total number of leukocytes per gram liver (*A*), and frequencies of DCs (*B*), cDC subsets (*C*) and CD4 T cells (*D*) were determined. (**E-F**) Hepatic leukocytes were restimulated with PMA/ionomycin in the presence of Brefeldin A for detection of intracellular cytokines. Abundance of FOXP3$^+$ Tregs (*E*), IL-5$^+$ Th2 cells and IL-17A$^+$ Th17 cells (*F*) were determined as frequencies of total leukocytes. Data shown are a pool of two independent experiments. Results are expressed as means ± SEM. * P<0.05 vs CD11c^{WT} (n = 4-8 mice per group). Related to figure 4.
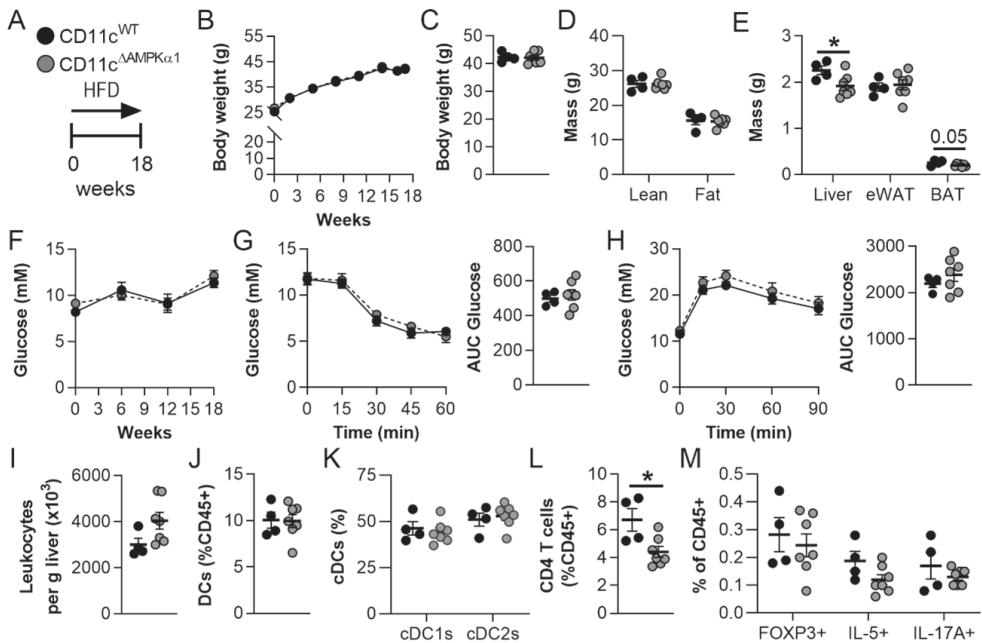
Supplementary Figure 7. Deletion of AMPKα1 from DCs did not recapitulate the immunometabolic phenotype of CD11cΔLKB1 mice. (**A**) CD11cWT (black symbols) and CD11cΔAMPKα1 mice (grey symbols) were fed a HFD for 18 weeks. (**B-C**) Body weight was monitored throughout the experiment. (**D-E**) Body composition (*D*) and weights of liver, eWAT and BAT (*E*) were measured at the end of the experiment. (**F**) Fasting blood glucose was measured at the indicated weeks. (**G**) An i.p. insulin tolerance test was performed 1 week before sacrifice and AUC calculated. (**H**) An i.p. glucose tolerance test was performed 1 week before sacrifice and AUC calculated. (**I-L**) At sacrifice, liver was collected and immune cells isolated. Total leukocytes per gram liver were quantified (*I*). Percentages of DCs (*J*), cDC subsets (*K*) and CD4 T cells (*L*) were determined by flow cytometry. (**M**) Liver leukocytes were restimulated with PMA and ionomycin in the presence of Brefeldin A for intracellular cytokine detection. Percentages of FOXP3+ Treg, IL-5+ Th2 and IL-17A+ Th17 cells were determined as frequencies of total leukocytes. Results are expressed as means ± SEM. * P<0.05 vs CD11cWT (n = 4-7 mice per group).
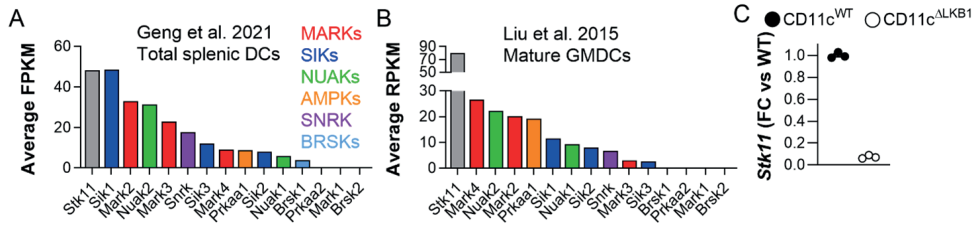
Supplementary Figure 8. Transcriptional analysis of LKB1 and its substrates in DCs. (**A-B**) Expression of *Stk11* (encoding LKB1) and its downstream targets *Mark1-4*, *Sik1-3*, *Nuak1-2*, *Prkaa1-2* (encoding AMPKα1-2), *Snrk* and *Brsk1-2* in total splenic DCs (Geng et al., *Immunology.* 2021; *A*) and mature GM-CSF-elicited bone marrow DCs (GMDCs; Liu et al., *J. Immunol.* 2015; *B*). (**C**) *Stk11* expression in GMDCs from CD11c[WT] (black symbols) and CD11c[ΔLKB1] mice (open symbols) at day 10 of culture. Related to figure 5.

5